Spectral quasi-linearization method for entropy generation using the Cattaneo-Christov heat flux model

Hiranmoy Mondal* and Precious Sibanda

School of Mathematics, Statistics and Computer Science, University of KwaZulu-Natal, Private Bag X01, Scottsville, Pietermaritzburg-3209, South Africa

*Presenting and Corresponding author: hiranmoymondal@yahoo.co.in

Abstract

In this paper, we study entropy generation in Sikiadas nanofluid flow along a moving plate subject to an inclined magnetic field and a Cattaneo-Christov heat flux model that may predict the effects of thermal relaxation time in the boundary layer flow. The nonlinear transport equations are solved using a spectral-quasi linearization method. An analysis of the convergence of the method is presented, and the importance of various fluid and physical parameters on the behavior of the solutions is explored. It is shown that the method converges fast and gives accurate results. The results show that entropy generation increases with an increase in the Reynolds number.

Keywords**: Cattaneo-Christov heat flux model; inclined magnetic field; Nanofluid; SQLM.**

Introduction:

Heat transfer characteristics in a fluid have traditionally been studied using Fourier's law of heat conduction. It is important in many industrial and engineering processes including nuclear reactor cooling, space cooling, energy production, biomedical applications such as magnetic drug targeting, heat conduction in tissues etc. and many others. The temperature difference between two unlike bodies causes heat transfer mechanism. The heat transfer phenomenon was primarily described by Fourier [1] which is parabolic energy equation for temperature field. One of the major shortcomings of this model is that it produces a parabolic energy equation which means that an initial disturbance would instantly affect the system under consideration. After that Cattaneo [2] modifies the Fourier law of heat conduction in which he added the thermal relaxation term. The addition of thermal relaxation time causes heat transportation in the form of thermal waves with finite speed. A material invariant formulation of the Cattaneo's model was presented by Christov [3] through the consideration of Oldroyd's upper-convected derivative. The Cattaneo-Christov equations uniqueness and structural stability were discussed by Ciarletta and Straughan [4]. Mushtaq et.al [5] were studied Sakiadis flow of UCM fluid by considering Cattaneo–Christov heat flux model and concluded that temperature distribution is Non-Monotonic with an increasing thermal relaxation time. Han [6] explored the heat transfer phenomenon of viscoelastic fluid under the Cattaneo–Christov theory and Salahuddin et.al [7] analysed the MHD flow of Williamson fluid with variable thickness by considering Cattaneo–Christov heat flux model.

The addition of nano-sized metallic or metal oxide particles to base fluids such as oil or water leads to nanofluids. These fluids have enhanced thermo physical properties such as a higher thermal conductivity, viscosity, thermal diffusivity and convective heat transfer coefficients compared to base fluids. Dogonchi and Ganji [8] investigated the importance of the Cattaneo–Christov heat flux model for heat transfer in an MHD nanofluid flow between parallel plates. Sithole et al. [9] investigated entropy generation in a second grade fluid flow over a stretching sheet.

The innovation of our study in heat transfer fluids involves the addition of nano-sized metallic or metal oxide particles to base fluids such as oil or water. The resulting nanofluids have been found to possess enhanced thermo physical properties such as the thermal conductivity, viscosity, thermal diffusivity and convective heat transfer coefficients compared to the of base fluid. These novel properties ensure that nanofluids have great potential for useful as heat transfer fluids, in, for instance, microelectronic devices, fuel cells, engine cooling/vehicle thermal management, heat exchangers and in boiler flue gas temperature reduction. The boundary layer flow of a third-grade viscoelastic power-law non-Newtonian fluid over a porous wedge was investigated by Rashidi et al. [10]. He studied the impact of buoyancy and thermal radiation on magneto hydrodynamic nanofluid flow past a stretching sheet. Khan and Pop [11] obtained a numerical solution for the two-dimensional flow of nanofluid over a linearly stretching sheet. Buongiorno [12] presented a nonhomogeneous equilibrium mathematical model for convective transport in nanofluids. Kuznetsov and Nield [13] studied the nanofluid boundary layer flow past a vertical plate. De et al. [14] were investigate the flow of nanofluids. She concluded that Brownian motion and thermophoretic diffusion of nanoparticles are the most important mechanisms for the abnormal convective heat transfer enhancement.

The aim is to explore entropy generation and heat transfer characteristics in an MHD fluid flow for the well-known Sakiadis problem and a Maxwell nanofluid using the Cattaneo–Christov heat flux model. The conservation equations are solved numerically using the spectral quasilinearization method. The significance of physical and fluid parameters on the flow and entropy generation fields is discussed in detail.

Mathematical formulation:

The plate is assumed to be at a constant temperature Tw and T∞ denotes the ambient fluid temperature. Christov's heat flux model is used. The uniform magnetic field is applied at an angle $\wedge$ to the positive direction of the y−axis. Making use of the standard boundary layer approximations, the equations governing the steady incompressible flow of nanofluid and heat transfer can be expressed as below:

$$\frac{\partial u}{\partial x}+\frac{\partial v}{\partial y}=0 \tag{1}$$

$$u\frac{\partial u}{\partial x}+v\frac{\partial u}{\partial y}+\lambda_1\left(\frac{u^2\partial^2 u}{\partial x^2}+v^2\frac{\partial^2 u}{\partial y^2}+2uv\frac{\partial^2 u}{\partial x\partial y}\right)=\nu\frac{\partial^2 u}{\partial y^2}-\frac{\sigma}{\rho}B_0^2 sin^2(\wedge)u \tag{2}$$

$$\rho c_p\left(u\frac{\partial T}{\partial x}+v\frac{\partial T}{\partial y}\right)=-\nabla.\mathbf{q}+(\rho c_p)_f\left[D_B\frac{\partial C}{\partial y}\frac{\partial T}{\partial y}+\frac{D_T}{T_\infty}\left(\frac{\partial T}{\partial y}\right)^2\right] \tag{3}$$

$$u\frac{\partial C}{\partial x}+v\frac{\partial C}{\partial y}=D_B\frac{\partial^2 C}{\partial y^2}+\frac{D_T}{T_\infty}\frac{\partial^2 T}{\partial y^2} \qquad (4)$$

In the energy equation, **q** is the heat flux that satisfies the following equation

$$\mathbf{q}+\lambda_2\left(\frac{\partial \mathbf{q}}{\partial t}+V.\nabla\mathbf{q}-\mathbf{q}.\nabla V+(\nabla.V)\mathbf{q}\right)=-k\nabla T \qquad (5)$$

In which $V=(u,v,0)$ 2-Dimensional velocity vector, λ_2 is the relaxation time for heat flux and k is the thermal conductivity of the fluid. We considered flow is incompressible so that equation (5) takes the form as

$$\mathbf{q}+\lambda_2\left(\frac{\partial \mathbf{q}}{\partial t}+V.\nabla\mathbf{q}-\mathbf{q}.\nabla V\right)=-k\nabla T \qquad (6)$$

Eliminating $\mathbf{q}$ from equations (3) and (5), we obtain the following equation (for more details see Christov [25] and Han et al [28])

$$u\frac{\partial T}{\partial x}+v\frac{\partial T}{\partial y}+\lambda_2\left(\begin{array}{l}\left(u\frac{\partial u}{\partial x}+v\frac{\partial u}{\partial y}\right)\frac{\partial T}{\partial x}+\left(u\frac{\partial v}{\partial x}+v\frac{\partial v}{\partial y}\right)\frac{\partial T}{\partial y}\\ +u^2\frac{\partial^2 T}{\partial x^2}+v^2\frac{\partial^2 T}{\partial y^2}+2uv\frac{\partial^2 T}{\partial x\partial y}\end{array}\right)=\alpha\frac{\partial^2 T}{\partial y^2}+\tau\left[D_B\frac{\partial C}{\partial y}\frac{\partial T}{\partial y}+\frac{D_T}{T_\infty}\left(\frac{\partial T}{\partial y}\right)^2\right] \qquad (7)$$

In addition, the boundary conditions are

$$u=U,\quad v=0,\quad T=T_w,\quad D_B\frac{\partial C}{\partial y}+\frac{D_T}{T_\infty}\frac{\partial T}{\partial y}=0\quad at\quad y=0 \qquad (8)$$

$$u\to 0,\quad T\to T_\infty,\quad C\to C_\infty\qquad as\quad y\to\infty \qquad (9)$$

where x, y are the coordinates along plate and normal to the plate respectively, u, v are velocity components of along x and y axis respectively, λ_1 is the relaxation time of the fluid, c_p is the specific heat , ρ is the density of the fluid, ν is the kinematic viscosity, D_B and D_T is the Brownian diffusion coefficient and thermophoretic diffusion coefficient respectively. $\tau=\frac{(\rho c)_p}{(\rho c)_f}$ is the ratio between the effective heat capacity of the nanoparticles material and heat capacity of the fluid, T and C are fluid temperature and nanoparticles fraction, respectively, T_w and T_∞ are the temperature of the fluid at the wall and ambient temperature.

Introducing the following similarity transformations

$$\eta=y\sqrt{\frac{U}{\nu x}},\qquad u=Uf'(\eta),\qquad v=-\sqrt{\frac{U\nu}{x}}(f-\eta f'),\theta(\eta)=\frac{T-T_\infty}{T_w-T_\infty},\qquad \phi(\eta)=\frac{C-C_\infty}{C_\infty} \qquad (10)$$

By using similarity transformations equations (1), (2), (4) and (6) reduces to

$$f'''+\frac{1}{2}ff''-\frac{\beta_1}{2}\left(2ff'f''+f^2f'''+\eta f'^2f''\right)-Msin^2(\wedge)f'=0 \qquad (11)$$

$$\frac{1}{Pr}\theta''+\frac{1}{2}f\theta'-\frac{\beta_2}{2}\left(3ff'\theta'+f^2\theta''\right)+Nb\theta'\phi'+Nt\theta'^2=0 \qquad (12)$$

$$\phi'' + \frac{1}{2} LePrf\,\phi' + \frac{Nt}{Nb}\theta'' = 0 \tag{13}$$

and the boundary conditions are

$$f' = 1, \quad f = 0, \quad \theta = 1, \quad Nb\phi' + Nt\theta' = 0 \quad at \quad \eta = 0 \tag{14}$$

$$f' \to 0, \quad \theta \to 0, \quad \phi \to 0 \quad as \quad \eta \to \infty. \tag{15}$$

Here $M = \frac{\sigma B_0^2}{\rho U}$ is the magnetic parameter, $\wedge$ is the inclined angle, $\beta_1 = \frac{U\lambda_1}{2x}$ is the viscoelastic fluid parameter, $\beta_2 = \frac{U\lambda_2}{2x}$ is the dimensionless thermal relaxation time, $Pr = \frac{\nu}{\alpha}$ is the Prandtl number, $Nb = \frac{\tau D_B C_\infty}{\nu}$ is the Brownian motion parameter, $Nt = \frac{\tau D_T (T_w - T_\infty)}{T_\infty \nu}$ thermophoresis parameter and $Le = \frac{\nu}{D_B}$ is the Lewis number.

Entropy Generation:

The volumetric entropy generation in the Cattaneo-Christov nanofluid, which is based on the second law of thermodynamics, is given by

$$S_{gen}''' = \frac{k_f}{T_\infty^2}\left(\frac{\partial T}{\partial y}\right)^2 + \frac{\sigma B_0^2}{T_\infty} u^2 + \frac{R\,D_B}{T_\infty}\frac{\partial T}{\partial y}\frac{\partial C}{\partial y} + \frac{RD_B}{C_\infty}\left(\frac{\partial C}{\partial y}\right)^2 \tag{16}$$

It is suitable to define the entropy generation number N_G as a ratio between the local volumetric entropy generation rate S_{gen}''' and a characteristic rate of entropy generation which is defined by S_0'''

$$S_0''' = \frac{k_f (T_w - T_\infty)}{T_\infty^2 x^2} \tag{17}$$

The entropy generation number N_G can be obtained as

$$N_G = \frac{S_{gen}'''}{S_0'''} = \mathrm{Re}\,\theta'^2 + \frac{\mathrm{Re}\,Br\,M}{\chi} f'^2 + \frac{\mathrm{Re}\sum}{\chi}\theta'\phi' + \frac{\mathrm{Re}\sum}{\chi^2}\phi'^2 \tag{18}$$

Where Re is the Reynolds number, Br is the Brinkman number, $\sum$ is the constant and χ is the temperature difference parameter.

Equation (18) can be obtained as a summation of the entropy generation number caused by the heat transfer ($N1$) and the entropy generation number caused by both diffusive irreversibility and magnetic field ($N2$). That is $N_G = N1 + N2$, where

$$N1 = \mathrm{Re}\,\theta'^2, \quad N2 = \frac{\mathrm{Re}\,Br\,M}{\chi} f'^2 + \frac{\mathrm{Re}\sum}{\chi}\theta'\phi' + \frac{\mathrm{Re}\sum}{\chi^2}\phi'^2 \tag{19}$$

The heat transfer irreversibility, diffusive irreversibility and the magnetic field all contribute to entropy generation. It is therefore worthwhile investigating the conditions under which heat transfer dominates entropy generation. To investigate this question, the Bejan (*Be*) number is defined as the ratio of entropy generation due to heat transfer and the entropy generation number.

$$Be = \frac{N1}{N_G} \tag{20}$$

The Bejan number takes values in range [0, 1]. At the extreme when $Be = 1$ the irreversibility of heat transfer dominates. On the other extreme when $Be = 0$ the combined effects of diffusion and magnetic field dominates the irreversibility. When $Be = 0.5$, the contribution of heat transfer in entropy generation is the same as the combined contribution of diffusion and magnetic field in entropy generation. Additionally, the Bejan number *Be* is considered at the best values of the parameters at which the entropy generation its minimum.

Method of solution:

The nonlinear-coupled ordinary differential equations (11)-(13) subject to the boundary conditions (14) have been solved numerically using the spectral quasi linearization method (SQLM). The quasi linearization method is employed to linearize the equations before they are solved iteratively using the Chebyshev spectral collocation method. Applying the quasi linearization procedure to equations (11)-(15), the resultant equations are

$$\alpha_{1,r} f'''_{r+1} + \alpha_{2,r} f''_{r+1} + \alpha_{3,1} f'_{r+1} + \alpha_{4,r} f_{r+1} \quad = R_1 \tag{21}$$

$$\beta_{1,r} f_{r+1} + \beta_{2,r} f'_{r+1} + \beta_{3,r}\theta''_{r+1} + \beta_{4,r}\theta'_{r+1} + \beta_{5,r}\phi'_{r+1} = R_2 \tag{22}$$

$$\gamma_{1,r} f_{r+1} + \gamma_{2,r}\theta''_{r+1} + \gamma_{3,r}\phi''_{r+1} + \gamma_{4,r}\phi'_{r+1} \quad = R_3 \tag{23}$$

and the boundary conditions are

$$f_{r+1} = 0, \quad f'_{r+1} = 1, \ \theta_{r+1} = 1, \ Nb\phi'_{r+1} + Nt\theta'_{r+1} = 0, \ \text{ at } \eta = 0$$

$$f'_{r+1} = 0, \quad \theta_{r+1} = 0, \ \phi_{r+1} = 0 \ \text{ at } \eta \to \infty. \tag{24}$$

Where

$$\alpha_{1,r} = \left(\frac{1}{2} f''_r - \beta_1 f'_r f''_r - \beta_1 f_r f'''_r\right), \quad \alpha_{2,r} = -\beta_1 \eta f'_r f''_r - \beta_1 f_r \ f''_r - M\sin^2(\Lambda),$$

$$\alpha_{3,r} = -\beta_1 f_r f'_r - \frac{\beta_1}{2}\eta f_r'^2 + \frac{1}{2} f_r, \quad \alpha_{4,r} = 1 - \frac{\beta_1}{2} f_r^2$$

$$\beta_{1,r} = \frac{1}{2}\theta'_r - \frac{\beta_2}{2}(3 f'_r\theta'_r + 2 f_r\theta''_r), \ \beta_{2,r} = -\frac{3\beta_2}{2} f_r\theta'_r, \ \beta_{3,r} = \frac{1}{\Pr} - \frac{\beta_2}{2} f_r^2,$$

$$\beta_{4,r} = \frac{1}{2} f_r - \frac{3\beta_2}{2} f_r f'_r + Nb\phi'_r + 2Nt\theta'_r, \qquad \beta_{5,r} = Nb\theta'_r$$

$$\gamma_{1,r} = \frac{1}{2} PrLe\phi_r^{'}, \ \gamma_{2,r} = \frac{Nt}{Nb}, \quad \gamma_{3,r} = 1, \quad \gamma_{4,r} = \frac{1}{2} PrLef_r$$

$$R_1 = \frac{1}{2} f_r^{'} f_r^{''} - \beta_1 (f_r^2 f_r^{'''} + \eta f_r^{'2} f_r^{''} + 2 f_r \ f_r^{'} f_r^{''})$$

$$R_2 = \frac{1}{2} f_r \theta_r^{'} + Nt\theta_r^{'2} + Nb\theta_r^{'}\phi_r^{'} - \beta_2 (3 f_r f_r^{'}\theta_r^{'} + f_r^2 \theta_r^{''})$$

$$R_3 = \frac{1}{2} PrLef_r \phi_r^{\prime}$$

The equations (21) to (24) constitutes a linear system of coupled differential equations with variable coefficients and can be solved iteratively using any numerical method for r = 1, 2, 3.... In this work, as we discussed below, the Chebyshev spectral collocation method was used to solve the QLM scheme (21) to (24). Before applying the spectral method, it is convenient to transform the domain in the η direction is approximated to [0, L] where L is the edge of the boundary limit (large enough), use the transformation of algebraic mapping $\eta = \frac{(\tau+1)L}{2}$ to map the physical domain into the computational domain [-1, 1]. This basic idea of this method is approximating the unknown functions by the Chebyshev interpolating polynomials in such a way that they are collocated at the Gauss-Lobatto points defined as

$$\tau_i = \cos(\frac{\pi i}{N}), \quad -1 \le \tau \ge 1, \quad i = 0,1,2,\dots,N \tag{25}$$

where N is the number of collocation points. The derivative of f_{r+1} at the collocation points is represented as

$$\frac{\partial^p f_{r+1}}{\partial \eta^p} = \left(\frac{2}{L}\right)^p \sum_{k=0}^{N} D_{N,k}^p f_{r+1}(\tau_k) = \mathbf{D}^p \mathbf{F} \tag{26}$$

where $\mathbf{D} = \frac{2}{L} D$ and D is the Chebyshev spectral differentiation matrix $\mathbf{F} = [f(\tau_0), f(\tau_1), ... f(\tau_N)]$. Similarly the derivatives of θ, and ϕ given by $\theta^p = \mathbf{D}^p \Theta \quad \phi^p = \mathbf{D}^p \Phi$. $\theta^p = \mathbf{D}^p \Theta \quad \phi^p = \mathbf{D}^p \Phi$. where p is the order of derivative, and $\mathbf{D}$ is the matrix of order $(N+1)\times(N+1)$. Substituting (24)-(25) into the equations (21)-(23) we obtain

$$\left[\boldsymbol{\alpha}_{1,r}\mathbf{D}^3 + \boldsymbol{\alpha}_{2,r}\mathbf{D}^2 + \boldsymbol{\alpha}_{3,r}\mathbf{D} + \boldsymbol{\alpha}_{4,r} \right] \mathbf{F}_{r+1} = \mathbf{R}_1 \tag{27}$$

$$\left[\boldsymbol{\beta}_{1,r}\mathbf{D} + \boldsymbol{\beta}_{2,r}\mathbf{I} \right] \mathbf{F}_{r+1} + \left[\boldsymbol{\beta}_{3,r}\mathbf{D}^2 + \boldsymbol{\beta}_{4,r}\mathbf{D} \right] \boldsymbol{\Theta}_{r+1} + \left[\boldsymbol{\beta}_{5,r}\mathbf{D} \right] \boldsymbol{\Phi}_{r+1} = \mathbf{R}_2 \tag{28}$$

$$\left[\boldsymbol{\gamma}_{1,r}\mathbf{I}\right]\mathbf{F}_{r+1}+\left[\boldsymbol{\gamma}_{2,r}\mathbf{D}^2\right]\boldsymbol{\Theta}_{r+1}+\left[\boldsymbol{\gamma}_{3,r}\mathbf{D}^2+\boldsymbol{\gamma}_{4,r}\mathbf{D}\right]\boldsymbol{\Phi}_{r+1}=\mathbf{R}_3 \tag{29}$$

Applying spectral method on the boundary conditions gives

$$f_{r+1}(\tau_N)=0,\quad \sum_{k=0}^{N} D_{N,k} f_{r+1}(\tau_k)=1,\quad \theta_{r+1}(\tau_N)=1,\quad Nb\sum_{k=0}^{N} D_{N,k}\phi_{r+1}(\tau_k)+Nt\sum_{k=0}^{N} D_{N,k}\theta_{r+1}(\tau_k)=0$$

$$\sum_{k=0}^{N} D_{0,k} f_{r+1}(\tau_k)=0,\quad \theta_{r+1}(\tau_0)=0,\quad \phi_{r+1}(\tau_0)=0 \tag{30}$$

The above system of equations is written in the matrix form as

$$\begin{bmatrix} A_{11} & A_{12} & A_{13} \\ A_{21} & A_{22} & A_{23} \\ A_{31} & A_{32} & A_{33} \end{bmatrix}\begin{bmatrix} \mathbf{F}_{r+1} \\ \boldsymbol{\Theta}_{r+1} \\ \boldsymbol{\Phi}_{r+1} \end{bmatrix}=\begin{bmatrix} \mathbf{R}_1 \\ \mathbf{R}_2 \\ \mathbf{R}_3 \end{bmatrix} \tag{31}$$

Where

$$A_{11}=diag[\alpha_{1,r}]\mathbf{D}^3+diag[\boldsymbol{\alpha}_{2,r}]\mathbf{D}^2+diag[\boldsymbol{\alpha}_{3,r}]\mathbf{D}+diag[\boldsymbol{\alpha}_{4,r}]\mathbf{I}$$

$$A_{12}=\mathbf{0}\ ,\ A_{13}=\mathbf{0}$$

$$A_{21}=diag[\boldsymbol{\beta}_{1,r}]\mathbf{D}+diag[\boldsymbol{\beta}_{2,r}]\mathbf{I}\ ,$$

$$A_{22}=diag[\boldsymbol{\beta}_{3,r}]\mathbf{D}^2+diag[\boldsymbol{\beta}_{4,r}]\mathbf{D},$$

$$A_{23}=diag[\boldsymbol{\beta}_{5,r}]\mathbf{D}\ ,\ A_{31}=diag[\boldsymbol{\gamma}_{1,r}]\mathbf{I},$$

$$A_{32}=diag[\boldsymbol{\gamma}_{2,r}]\mathbf{D}^2,\ A_{33}=diag[\boldsymbol{\gamma}_{3,r}]\mathbf{D}^2+diag[\boldsymbol{\gamma}_{4,r}]\mathbf{D}$$

Where α, β and γ are $(N+1)\times(N+1)$ diagonal matrices, $\mathbf{I}$, $\mathbf{0}$ is a $(N+1)\times(N+1)$ Unit matrix and zero matrix respectively. The approximate solutions for $\mathbf{F}$, $\boldsymbol{\Theta}$ and $\boldsymbol{\Phi}$ are obtained by solving the matrix system (31).

Convergence analysis:

The coupled ordinary differential equation (11)–(13) with the boundary conditions (14)-(15) are solved using the SQLM. To validate the accuracy of the numerical results, the residual errors and the error norms are calculated. The residual error measures the extent to which the numerical solution approximates the genuine solution. The error norm is the difference between the approximate values at successive iterations and may be used to evaluate convergence and stability of the iteration scheme. We studied the change in the residual and error norms with several physical parameters such as the magnetic field, viscoelasticity, the thermal relaxation time, the Brownian motion and the thermophoresis parameter. The results are shown in Figs. 1 to 9.

Figs 1 to 3 show the residual errors in velocity profiles against iterations for different values of the magnetic field parameter, viscoelastic fluid and thermal relaxation time parameter. The residual errors converge after the fifth iteration with a residual error of 10^{-10}. The error norms decrease and smooth converge is achieved.

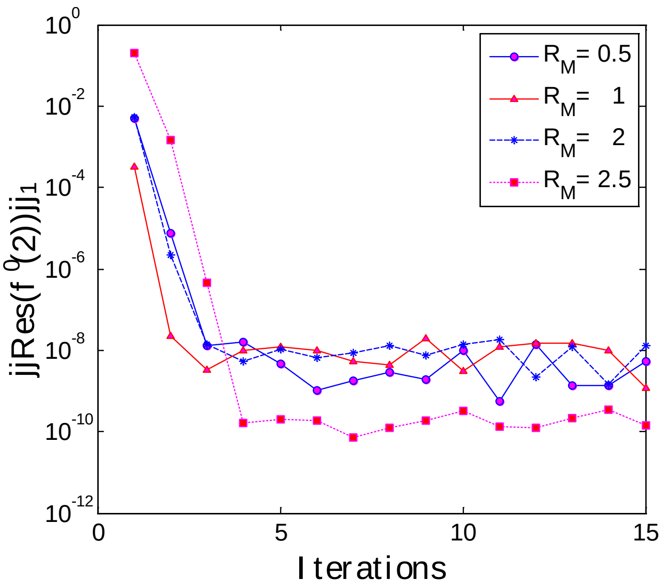

Fig.1: Residual error in the velocity profiles for different values of the magnetic parameter.

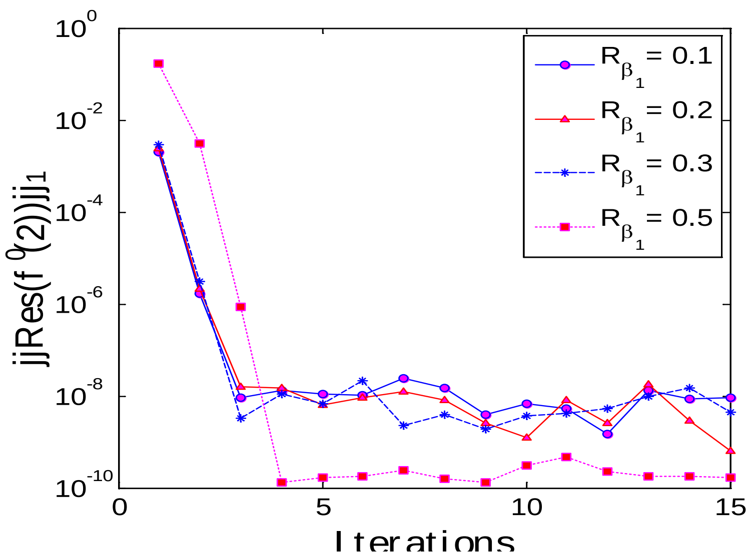

Fig. 2: Residual error in the velocity profiles for different values of β_1.

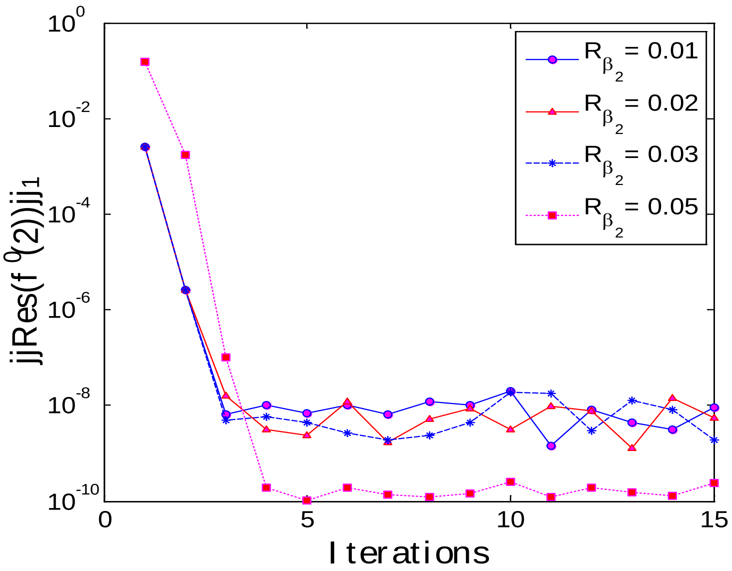

Fig.3: Residual error in the velocity profiles for different values of β_2.

Figs. 4 –5 show the residual errors and solution error norms against the number of iterations for different values of the thermal relaxation time and thermophoresis parameter. The residual errors converges after the fourth iteration with a residual error 10^{-10}. The solution error norm decreases and convergence is rapid.

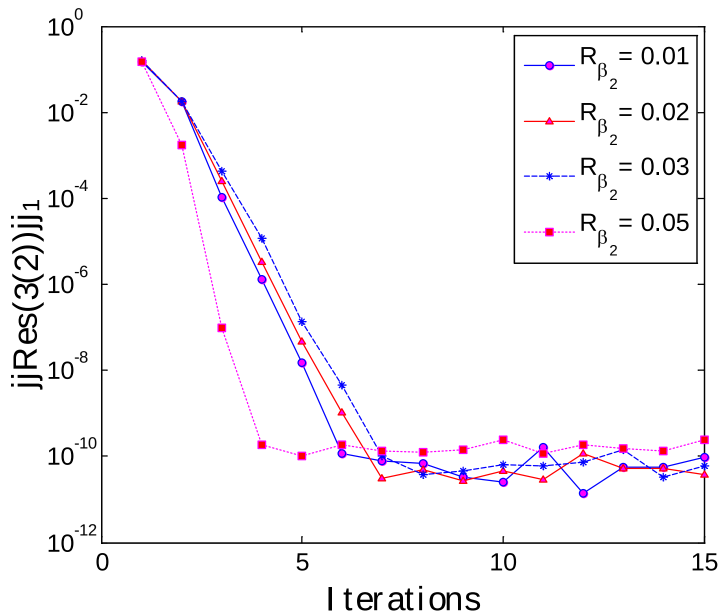

Fig.4: Residual error in the temperature profiles for different values of β_2.

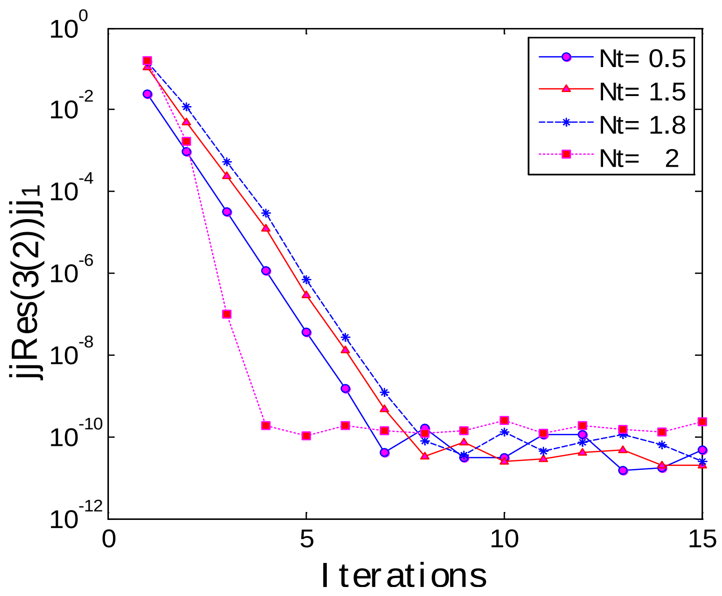

Fig.5: Residual error in the temperature profiles for different values of Nt.

Figs. 6-9 show the residual errors and solution error norms against iterations for different values of the viscoelastic fluid, dimensionless thermal relaxation time, Brownian motion and thermophoresis parameter. The residual errors converge after four iteration with a residual error is 10^{-10}.

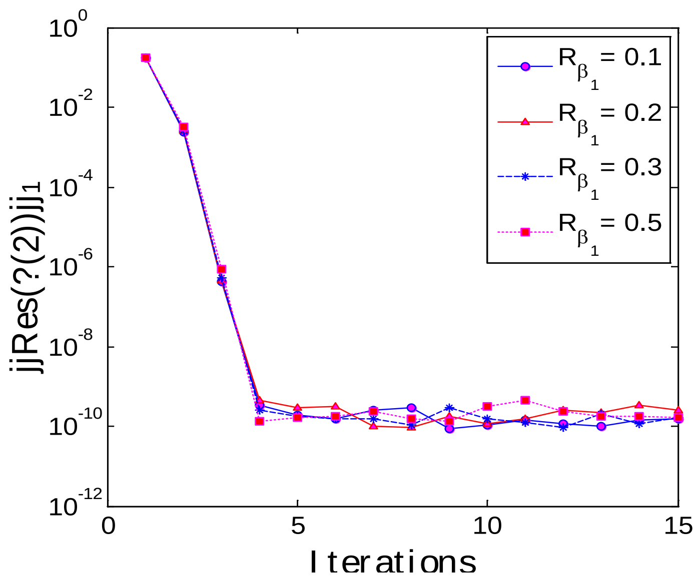

Fig.6: Residual error in concentration profiles for different values of β_1.

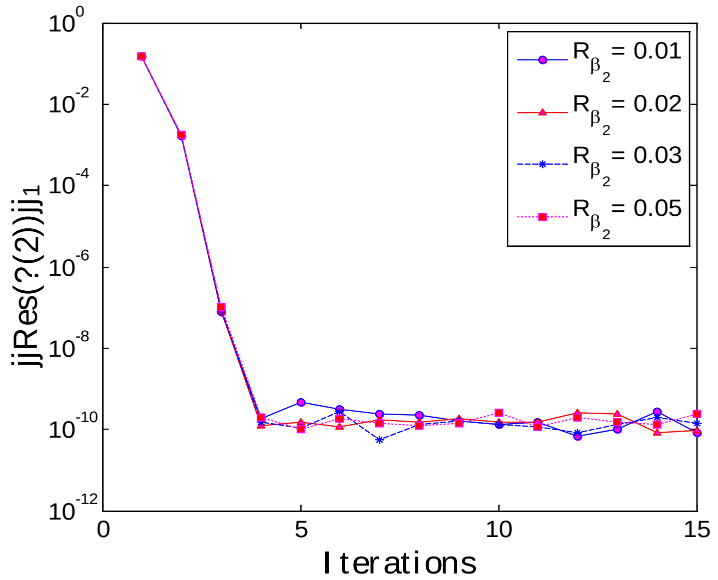

Fig.7: Residual error in concentration profiles for different values of β_2.

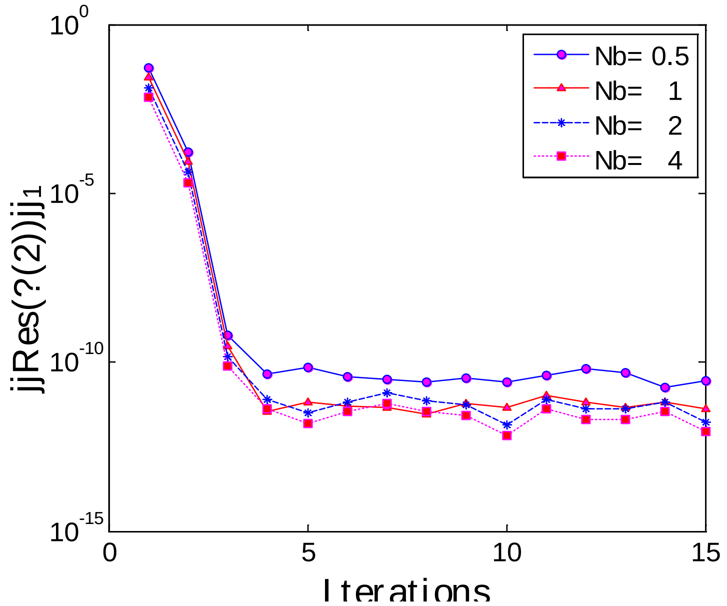

Fig.8: Residual error in concentration profiles for different values of Nb.

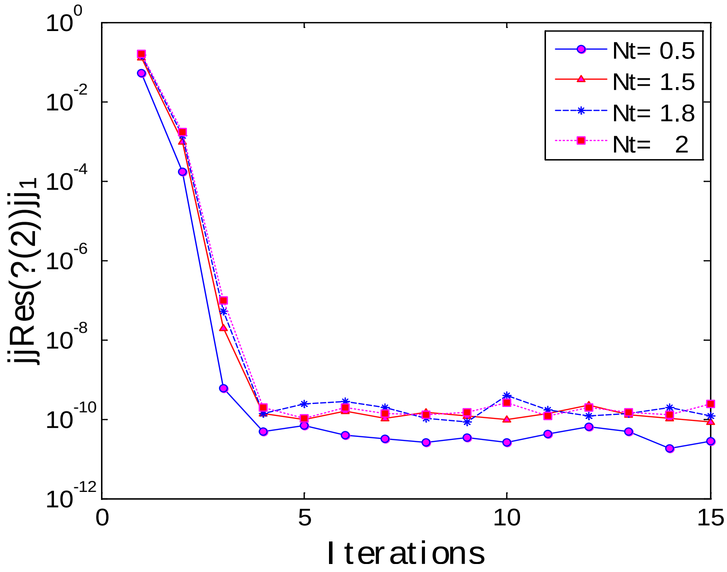

Fig.9: Residual error in concentration profiles for different values of Nt.

Fig. 10 shows the effect of the magnetic parameter on the entropy generation number. An increase in magnetic parameter results in an increase in entropy generation number. In the neighborhood of the sheet vicinity, the magnetic field has a significant impact on the entropy generation number. This tends to increase the resistance of the fluid motion, and consequently, the heat transfer rates. However, far from the sheet vicinity, the influence of magnetic parameter is insignificant.

Fig. 11 shows entropy generation with the Brinkman number, which represents a measure of the significance of the heat produced by viscous heating proportional to heat transported by molecular conduction. An increase in the Brinkman number tends to increase the entropy generation number especially near the sheet.

Fig. 12 shows the behavior of the entropy generation number with the temperature difference parameter. We observe that in the neighborhood of the sheet, the entropy generation number increases with the temperature difference parameter.

Fig. 13 relates the entropy generation number to the Reynolds number. We note that the Reynolds number has a significant impact on the entropy generation number as an increase in the Reynolds number leads to a significant increase in the entropy generation number, near the sheet. By increasing the Reynolds number, the fluid acceleration increases near the sheet.

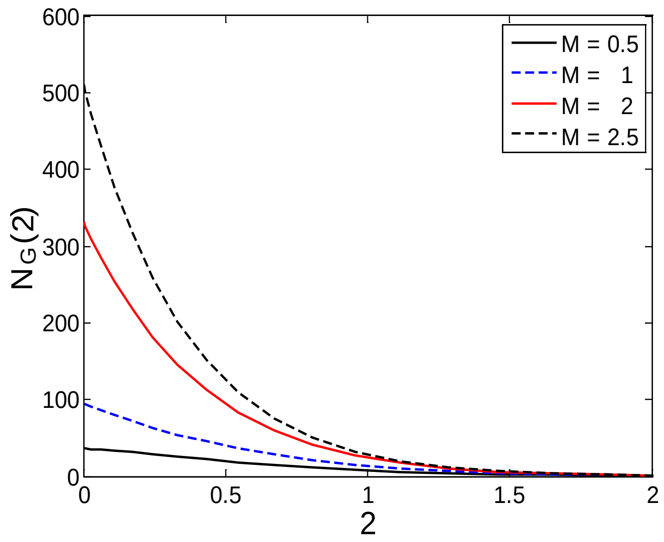

Fig. 10: Effects of the magnetic parameter on the entropy generation number N_G.

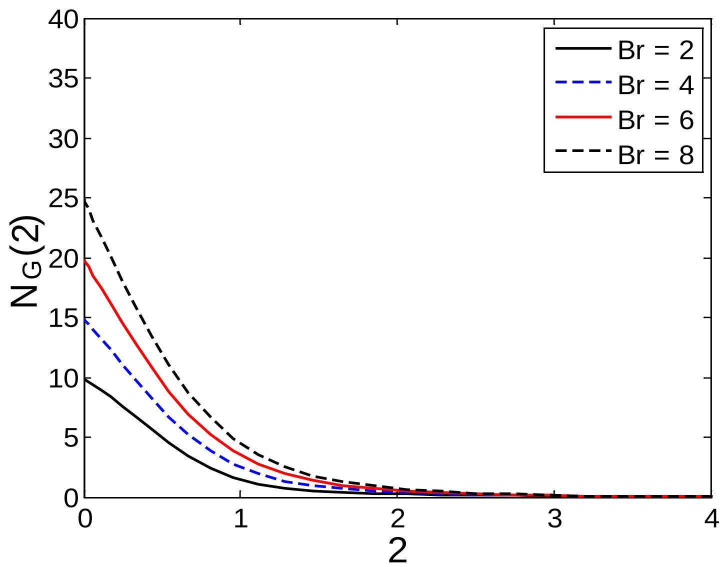

Fig. 11: Effects of Brinkman number on the entropy generation number N_G.

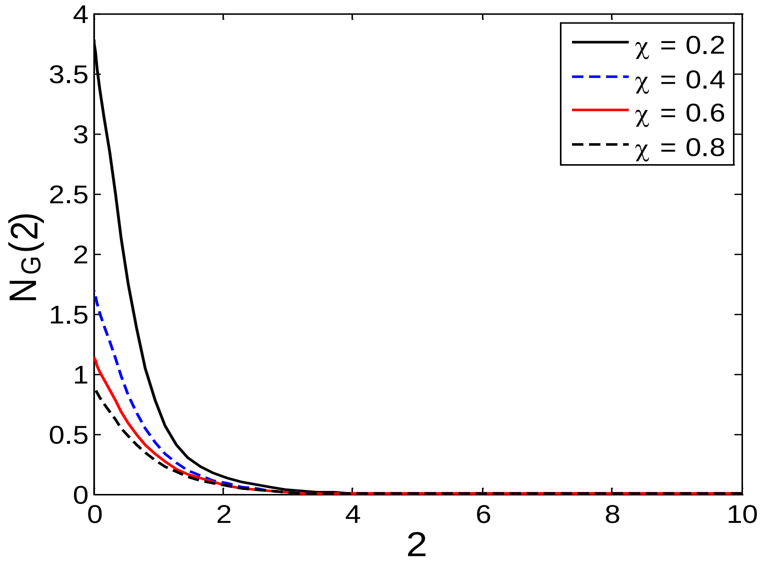

Fig. 12: Effects of temperature difference parameter on the entropy generation number N_G.

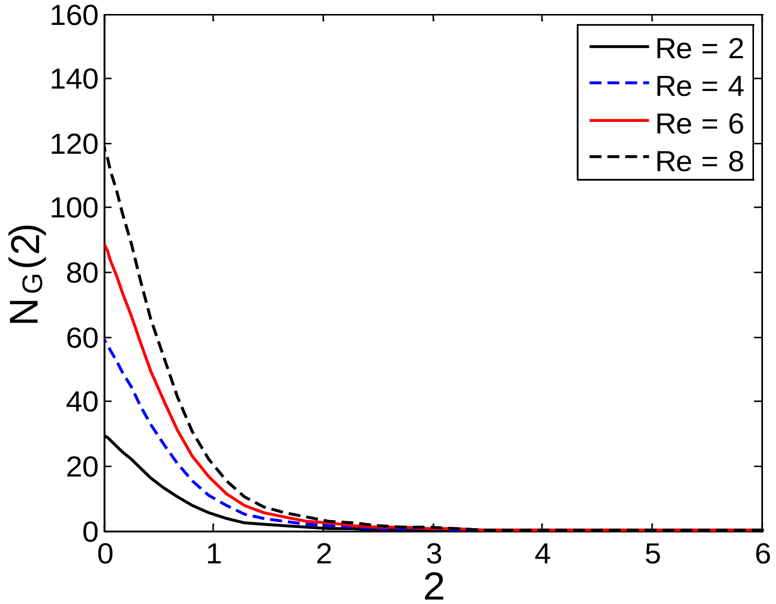

Fig. 13: Effects of Reynolds number on the entropy generation N_G.

Fig. 14 shows that the Bejan number is proportionally related to the magnetic parameter. As magnetic parameter increases, the entropy generation traced to diffusive irreversibility and magnetic field is totally controlled by the entropy generation due to heat transfer at the vicinity of the sheet. Figs.15 and 16 show the variations in the Bejan number with different values of the Brinkman number and the temperature difference parameter. We observe that an increase in the Brinkman number and temperature difference parameter leads to an increases in the Bejan number. An increase in the Brinkman number and the temperature difference parameter contribute to the increase in the magnitude of the diffusive irreversibility. However, the Brinkman number and the temperature difference parameter have no influence on heat transfer irreversibility. Consequently, the irreversibility ratio increases and the Bejan number decreases.

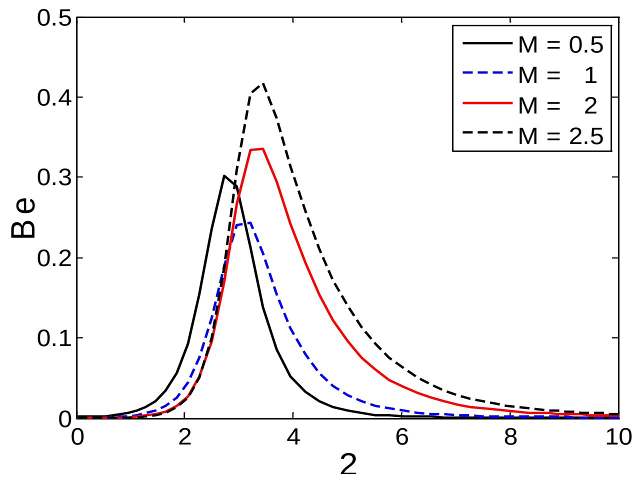

Fig.14: Effects of the magnetic parameter on the Bejan number (*Be*).

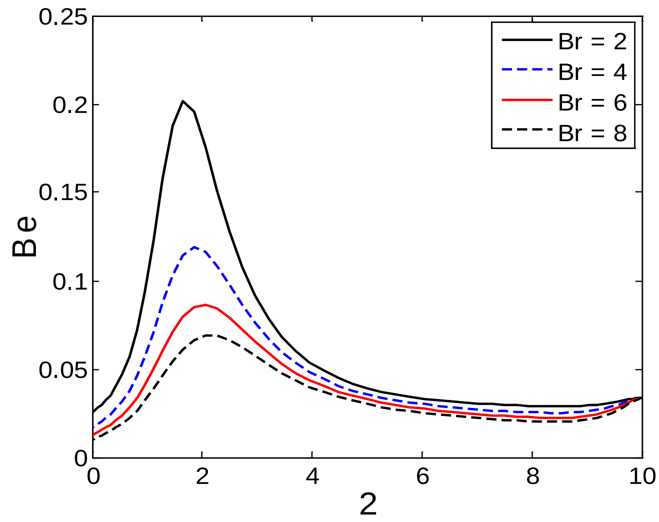

Fig.15: Effects of the Brinkman number on the Bejan number (*Be*).

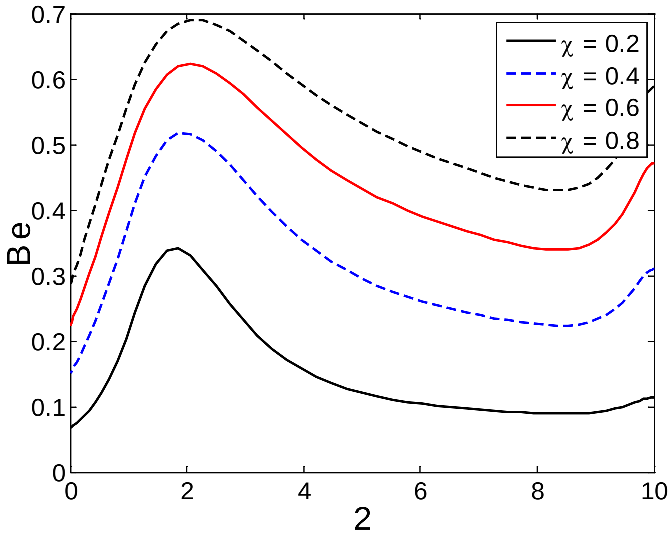

Fig. 16: Effects of temperature difference parameter on the Bejan number (Be).

Conclusions:

In this paper, we have investigated the influence of some fluid parameters on the entropy generation in Sakiadis nanofluid flow using Cattaneo-Christov heat flux model. The flow is over a stretching sheet subject to an inclined magnetic field. The transport equations were solved numerically using the spectral quasi-linearization method. The accuracy of the solutions was determined through an analysis of error norms and residual errors. Some key findings from the study include the following:

- The entropy generation number increases with an increase in temperature difference parameter, the Brinkman number and the Reynolds number.
- The Bejan number is strongly affected by variations in the temperature difference parameter and the Brinkman number.

Acknowledgment:

The authors would like to thanks Claude Leon Foundation Postdoctoral Fellowship, to the University of KwaZulu-Natal, South Africa, financially supported the research work.

References:

[1]. Fourier, J.B. J. Theorie analytique De La chaleur,Paris 1822.

[2]. Cattaneo C. (1948)Sulla conduzione del calore, Atti Semin. Mat. *Fis. Univ. Modena Reggio Emilia* **3,** 83–101.

[3]. Christov, C.I. (2009). On frame in different formulation of the Maxwell—Cattaneo model of finite-speed heat conduction. *Mechanics Research Communications* **36,** 481–486

[4]. Ciarletta M., Straughan, B. (2010). Uniqueness and structural stability for the Cattaneo—Christov equations. *Mechanics Research Communications* **37**: 445–447.

[5]. Mushtaq, A., Abbasbandy, S., Mustafa, M., Hayat, T. and Alsaedi A. (2016) Numerical solution for Sakiadis flow of upper-convected Maxwell fluid using Cattaneo-Christov heat flux model, *AIP Advances* **6**, 015-208.

[6]. Han S., Zheng, L., Li, C., and Zhang, X. (2014). Coupled flow and heat transfer in viscoelastic fluid with Cattaneo—Christov heat flux model. *Applied Mathematics Letters* **38**, 87–93

[7]. Salahuddin, T., Malik, M. Y., Hussain, A., Bilal, S., and Awais, M. (2016). MHD flow of Cattanneo–Christov heat flux model for Williamson fluid over a stretching sheet with variable thickness, *Journal of Magnetism and Magnetic Materials*, **401**, 991–997.
[8]. Dogonchi, A.S., Ganji, D.D. (2017) Impact of Cattaneo–Christov heat flux on MHD Nanofluid flow and heat transfer between parallel plates considering thermal radiation effect. *Journal of the Taiwan Institute of Chemical Engineers* **80,** 52–63.
[9] Sithole, H., Mondal,H., Sibanda, P. (2018) Entropy generation in a second grade magnetohydrodynamic nanofluid flow over a convectively heated stretching sheet with nonlinear thermal radiation and viscous dissipation. *Results in Physics* **9**, 1077–1085.
[10]. Rashidi, M.M., Ganesh, N.V., Hakeem, A.K.A., and Ganga, B. (2014)Buoyancy effect on MHD flow of nanofluid over a stretching sheet in the presence of thermal radiation, *Journal of Molecular Liquids*, 198, 234-238.
[11]. Khan W.A., Pop, I. (2010) Boundary-layer flow of a nanofluid past a stretching sheet. *International Journal of Heat and Mass Transfer* **53**, 2477–2483.
[12]. Buongiorno, J. (2006) Convective transport in nanofluids. *Journal of Heat Transfer* **128**(3):240–250.
[13]. Kuznetsov A.V., Nield, D.A. (2010) Natural convective boundary-layer flow of a nanofluid past a vertical plate. *Inernational Journal of Thermal Science* **49(2),** 243–247.
[14]. De,P., Mondal, H., and Bera, U.K. (2016) Dual solutions of heat and mass transfer of nanofluid over a stretching/shrinking sheet with thermal radiation. *Meccanica* **51(1),** 117-124.